EDMS 1396633

October 29, 2014

Feasibility study of BGI monitor for PS

Bernd Dehning, Oliver Keller, Emiliano Piselli, Mariusz Sapinski*,
Dominik Vilsmeier, Dominique Bodart
CERN CH-1211 Geneva 23, Switzerland

Keywords: Beam Gas Interaction, Ionization Profile Monitor

Summary

Beam Gas Ionization (BGI) monitor is used to measure the transverse beam profile. The electrons produced in the ionization process are guided by electric and magnetic fields to an electron detector. Currently the electron detection is based on phosphor screen with intensified cameras or multi-strip anodes. Both methods usually require amplification of the incoming electron flux by a Multi-Channel Plate (MCP). In this paper a new readout system, based on silicon pixel detector and not requiring MCP is studied for proposed, new BGI for CERN PS synchrotron. Other aspects: cage dimensions, field requirements, radiation conditions are presented as well.

*mail: mariusz.sapinski@cern.ch

Contents

1 Introduction

The Beam Gas Ionization monitor (BGI) uses electrons generated by beam interaction with the rest gas to estimate the transverse beam size [1]. The electrons are guided using electric field towards a sensitive element which registers their positions. In addition a magnetic field is applied in order to minimize the effect of the beam field on the electron motion and therefore to keep their transverse position close to the one where they were generated.

Here we describe a novel electron detection method based on silicon pixel detector bump-bonded to Timepix3 chip (hybrid pixel detector). We present that early digitization has many advantages and allows to readout the beam profiles with the frequency required by the PS operation. The hybrid silicon pixel detector technology development and popularization in the recent years allows to develop beam-instrumentation device with a reasonable budget.

2 Characterization of PS beams and vacuum

The parameters of the beam and vacuum in the possible locations of BGI are shown in Table 1. The evolution of optics functions and dispersion around the PS ring are shown in Fig. 1 and 2. For horozintal device a straight section with large β_x and small dispersion shall be chosen, therefore odd straight section (SD - section droite) is prefered. For vertical device the dispersion plays no role and an even SD shall be chosen.

parameter	value
β_x	12/22 m
β_y	22/12 m
pressure	$10^{-8} - 10^{-9}$ mbar
Horizontal dispersion	2.4-3.15 m
dp/p	10^{-3}
bunch length	3-205 ns
revolution time	$5.63 - 2.1\mu$s
kinetic energy	1.4 - 26 GeV (protons)
	15 - 1227 GeV (Pb^{54+})

Table 1: *General working conditions relevant for PS BGI monitor.*

The proposed locations are for the BGI are:

- SD31, 33, 35 - these location were excluded for the prototype installation due to high radiation environment,

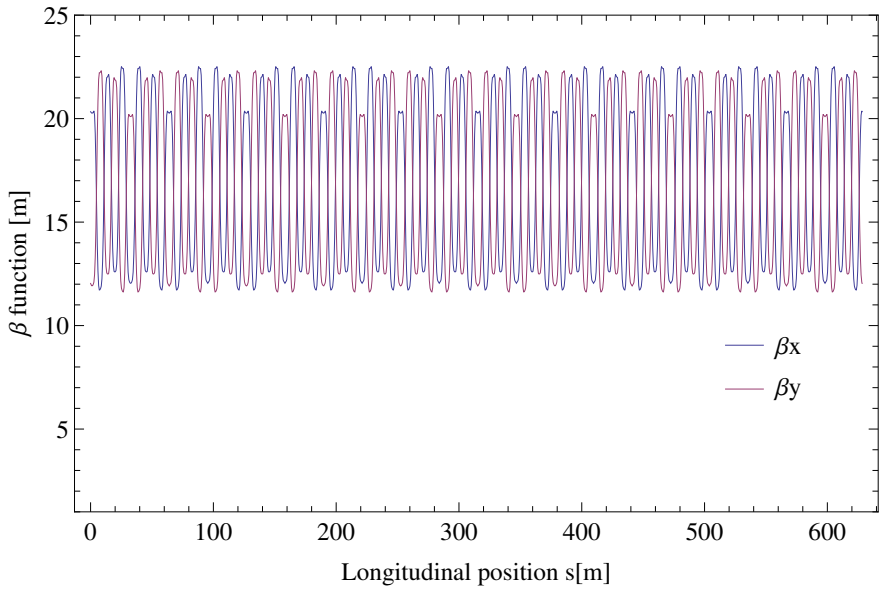

Figure 1: Optics functions of PS ring. *Courtesy S. Gilardoni.*

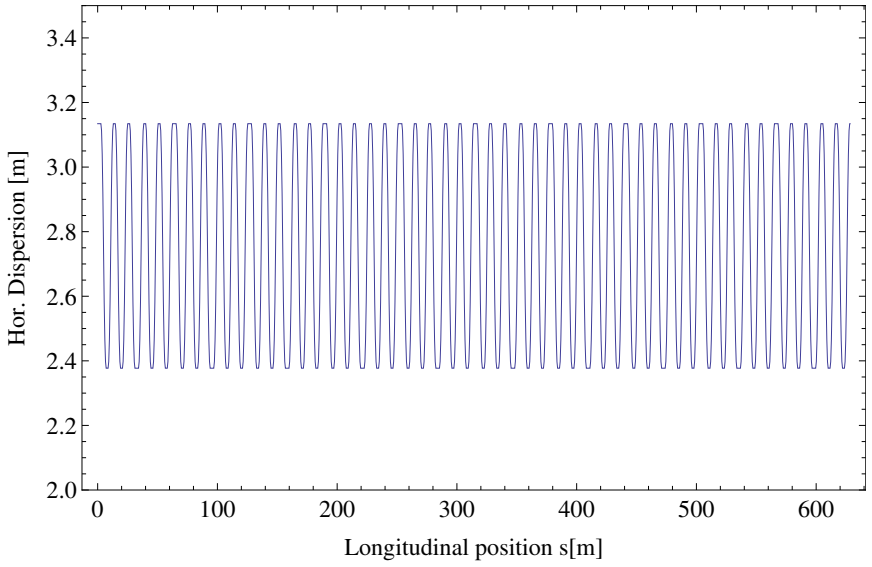

Figure 2: Dispersion in PS ring. *Courtesy S. Gilardoni.*

- SD21 - this location would be very good for horizontal device, but currently there is a CT kicker installed there and the decision to take it out will be taken later in 2015,
- SD82 (dcum 510-511 m) - this location has small horizontal beta (12 meters) so it would be optimal for vertical monitor.

The preliminary decision is to use SD82 to develop horizontal monitor, which shall have simpler construction due to significantly smaller vacuum chamber aperture.

2.1 Vacuum conditions

A good vacuum is an important parameter for PS, as very often in the same super-cycle it accelerates ions, and emittance of ion beam is easily affected by interaction with the rest gas. Figure 3 shows the gas pressure is SD82 during pumping after the vacuum has been opened during LS1. After switching on the sublimation pumps the pressure reaches levels below 10^{-9} mbar. The dynamic pressure, when high-intensity beam is in the machine, is not significantly higher because of short duration of PS cycle. In the further calculations the 10^{-9} mbar pressure level is assumed.

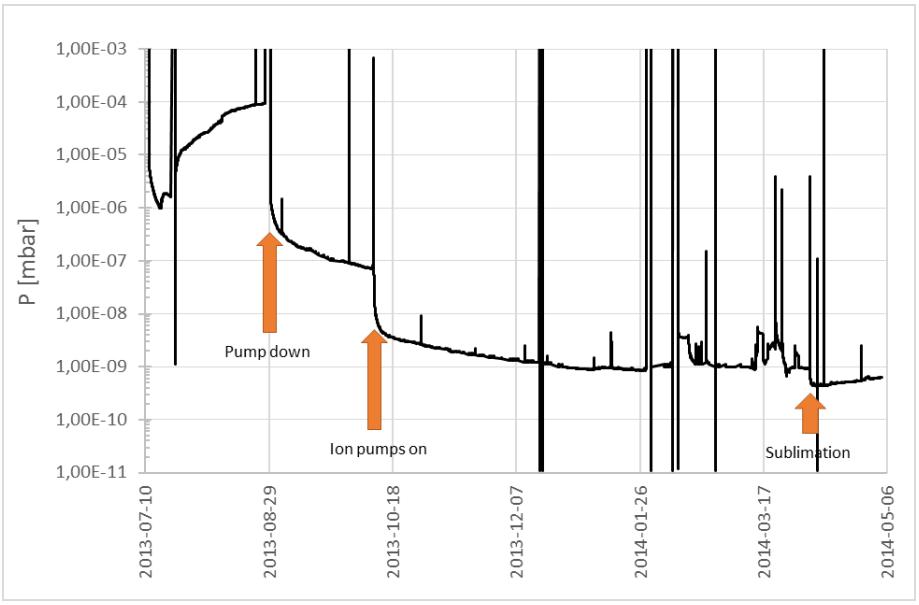

Figure 3: Vacuum evolution in SD82 during pumping after LS1. *Courtesy J. Ferreira.*

The signal levels in the BGI depend linearly on the gas pressure. It is shown later that for some beams the amount of electrons generated by a single bunch passage is too small to produce a profile. The creation of local gas pressure bump, as it is done in LHC where thanks to controlled injection the pressure reaches 10^{-8} mbar, could be a solution. One can immagine that this injection would be used only in particular conditions for instance for running period without ions in the machine.

2.2 Radiation levels

The radiation in the accelerator tunnel is due to the beam losses occuring for instance during injection and extraction of the beam and beam-gas interaction. None of this can be avoided. The mixed radiation field generated by these mechanisms contains the whole spectrum of particles: gamma, hadrons, neutrons and electrons. They affect electronics causing single event upsets in wich the state of the digital electronics is corrputed and a permanant radiation damage.
Figure 4

presents results of two studies: measurement of the activation 32 hours after the beam was stopped (red line) and the high-level dosimetry (HLD) measurements made during the run.

Regions with higher radiation levels are clearly identified and linked to equipment relevant for beam injection and extraction processes. These regions shall be avoided by the prototype installation of BGI, because of its sensitivity to high radiation levels.

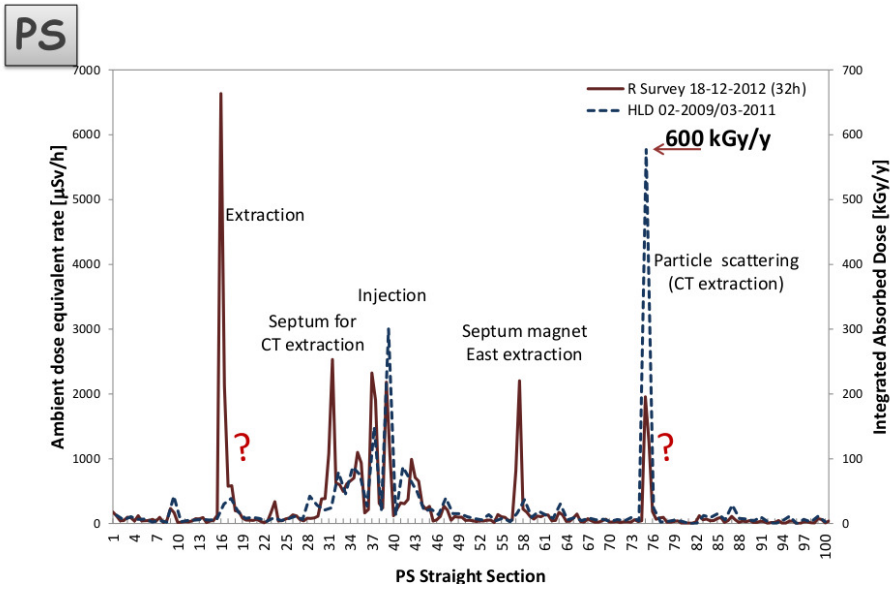

Figure 4: Monitoring of radiation in the PS.

In the regions with low radiation level the doses are still significant. A FLUKA simulation study has been performed for the SD01 (one of the low-radiation straight section), with a goal to estimate the attenuation of the yearly dose by a concrete shileding. Results of this simulation is shown in Fig. 5. The dose expected next to the beam, in the potential location of the BGI silicon sensor, exceeds 1 kGy/year. The location of data-acquisition electronics (FPGA) is about 1.5 meters from the beam. The region below the beamline is a good location. The expected dose is below 100 Gy/year, but with the proposed shielding the reduction is about tenfold: down to a few Gy/year.

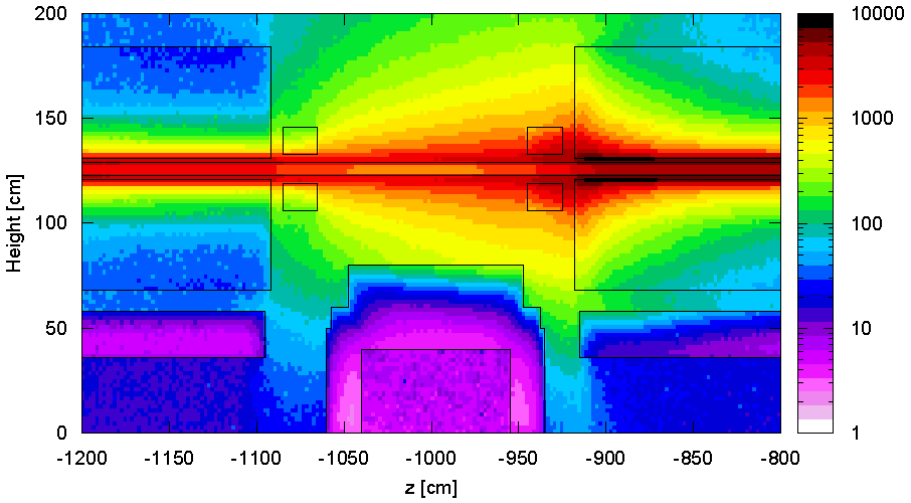

Figure 5: Simulation of yearly dose in low-radiation straight-section of PS. Dose units (color code) are Greys/year.

In order to better understand radiation environment in SD82, two RadMons were installed there in May 2014, in the assumed location of Timepix and FPGA.

3 Estimation of the signal

The BGI working principle is the detection of products of rest-gas ionization by the beam. Out of two possibilities: electrons or positive ions, the electrons are chosen. They are extracted from the beam and projected on a detector surface forming an image of the beam with electron density proportional to the beam density. The reason to chose electrons is a need for fast, bunch-by-bunch readout of the beam images. This is possible only with electrons which can travel the distance from the beam to the detector within about 2-4 ns, while ions, for the same distance, need about 400 ns.

The short time which electrons need to reach the detector is of course thanks to their small mass. On the other hand, for the same reason they are very sensitive to interactions with the bunch field. For high-charge bunches, as the ones in the PS, the profile may be significantly distorted. In order to avoid that a magnetic field along electric one is added. It confines electron movement in circles around the direction perpendicular to the detector.

3.1 Ionization cross-section

The ionization cross-section can be obtained from the Equation 1 originating from Bethe theory [2].

$$\sigma = 4\pi Z^2(\hbar/mc)^2\beta^{-2}(M_i^2 x + C_i) \quad (1)$$

In this equation Z is charge of the impacting beam particles, M_i and C_i are constans depending on gas type [3] (index i is there in case of gas mixture) and x is a variable depending only of speed of the impacting beam β:

$$x = ln[\beta^2/(1-\beta^2)] - \beta^2 \quad (2)$$

Example values of M_i and C_i can are shown in Table 2. In the last 4 columns the typical obtained ionization cross-sections are shown.

gas	M_i^2	C_i	cross-section [Mbar]			
			p 1.4 GeV	p 25 GeV	Pb54+ 15 GeV	Pb54+ 1227 GeV
Neon	2.02	18.2	0.44	0.56	5600	1350
Argon	4.22	37.93				
Hydrogen+Deuter	0.695	8.115	0.19	0.23	2650	570

Table 2: *Ionization cross-section for various gases.*

The ionization cross-section is very large. The influence of the gas type is rather small (factor 2-3).

Simulation with Geant 4 revealed similar, but more lower numbers. For instance for Pb^{54+} ions at 15.0 GeV interacting with Neon the number obtained is 830 Mbarn, while for 1227 GeV it is 510 Mbarn.

3.2 Ionization cross-section from Bethe-Bloch

One can attempt to evaluate ionization cross-section from Bethe-Bloch, although it is not a correct approach because Bethe-Bloch formula for dE/dx assumes multiple scattering and statistical interaction with dense matter with some electrons always nearby, while in the analyzed situation the gas density is very small.

The dE/dx of 1.4 GeV protons in a gas of normal density is about 2 MeV $\cdot$ cm^2/g. The gas density at pressure of 10^{-9}mbar can be calculated assuming ideal gas equation:

$$\rho = \rho_{STP} \cdot \frac{10^{-12}[bar]}{1[bar]} = 9 \cdot 10^{-4}[g/cm^3] \cdot 10^{-12} = 9 \cdot 10^{-16}[g/cm^3] \quad (3)$$

The energy left by the MIP over the detector (1.4 cm long) is:

$$\Delta E = 9 \cdot 10^{-16}[g/cm^3] \cdot 2[MeV cm^2/g] \cdot 1.4[cm] = 25.2 \cdot 10^{-16}\ MeV = 2.52 \cdot 10^{-9}\ eV \quad (4)$$

As the ionization energy is 21.56 eV (w-factor is 35 eV, but for low density ionization energy shall be used?). We could assume (but it is an assumption!) that probability for a proton to interact and ionize a gas atom is: P = $2.52 \cdot 10^{-16}$ eV/21.56 eV = $1.17 \cdot 10^{-17}$. From that the cross section is:

$$\sigma = P/N \tag{5}$$

where N is number of particles per unit of the gas target surface. This number we can get from number density multiplied by the target length l_{det} = 1.4 cm:

$$N = l_{det} \cdot pN_A/RT = 3.36 \cdot 10^{13}[1/m^2] \tag{6}$$

From above the cross-section is 3.5 mbarn. This is very different then cross-sections estimated in previous, correct method and the one estimated by Geant4 calculation.

Assumptions used for derivation of Bethe-Bloch relation are:

- Bethe-Bloch takes into account all elastic collistions with electrons and assumes free electrons,
- it assumes medium with an electron density large enough to provide interaction with several electrons every time,
- Bether-Bloch describes mean energy loss, assumes many soft collisions.

In general ionization cross section is dominated by rare hard collisions while the stopping power is dominated by many soft collisions. Therefore from Bethe-Bloch one cannot calculate ionization cross section.

Other subjects: ionization potential, influence of Stark/Zeeman effect,

3.3 Momenta of the produced electrons and space charge effect

The component of momentum of the produced electrons transverse to the magnetic field defines the radius of the electron trajectory around the magnetic field lines. This radius will affect the profile shape, therefore the knowledge of the electron momentum distribution is important [4].

On the other hand it has been found in LHC that the additional kick given to electrons due to the space charge effect of the beam can be large and more important than the initial momenta of electrons after ionization.

Simulations of both effects have been performed. In Figure 6 a deformation of low-emittance and high-intensity (the most difficult conditions in PS) beam profile is shown for magnetic field of 0.1 T. It can be concluded that the field of 0.2 T is sufficient for the future PS beams.

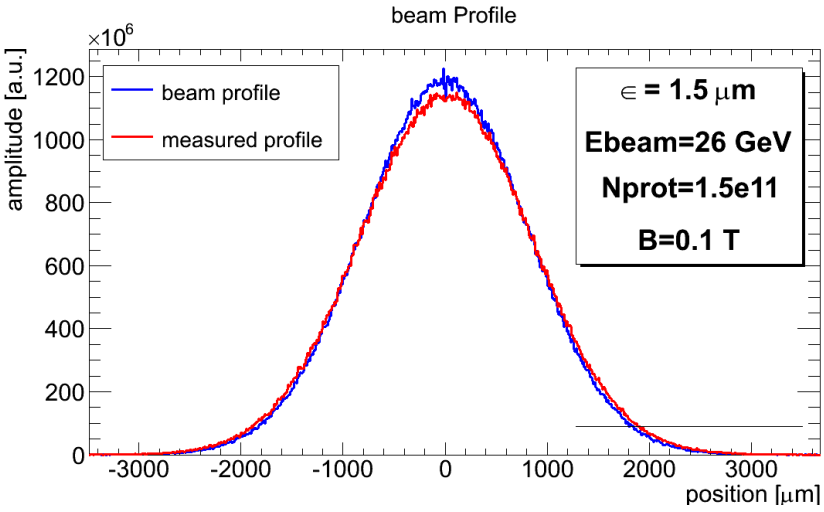

Figure 6: Registered beam profile deformation due to bunch space charge at PS for magnetic field of 0.1 T.

3.4 Electron production rates

The number of electrons produced by a single bunch and hitting the detector can be estimated from Equation 7:

$$n_e = l_{det}\sigma_{ion}N_b\frac{pN_A}{RT} \tag{7}$$

where:

- detector length $l_{det} = 1.4\ cm$ (see Timepix3 detector description chapter),
- σ_{ion} is given in Table 2 (optimistic case of Neon gas is chosen for subsequent calculations),
- N_b depends on the beam and is given in Table 3.

The component pN_A/RT is gas number density, with p = 10^{-9} mbar, N_A - Avogado contant, R- gas constant and $T = 300K$ - gas temperature. Note that there is no dependency on the beam size.

Table 3 shows beam parameters for the LHC beams in PS for various schemes. The beam size in the location of BGI is calculated assuming gaussian longitudinal distribution of the beam (see Equation 8) for two extreme cases:

- Horizontal monitor is SD82, i.e. in location with small horizontal beta and with (small) dispersion,
- Vertical monitor in SD82, i.e. in location with large vertical beta.

$$\sigma = \sqrt{\frac{\epsilon\beta}{\gamma} + D^2(\frac{dp}{p})^2} \tag{8}$$

beam type	bunch charge ($\cdot 10^{11}$)	particle type	bunch No	kinetic energy [GeV]	$\epsilon_{x,y}$ [μm]	bunch length [ns]	$\Delta p/p$ ($\cdot 10^{-3}$)	σ [mm] SD82 hor	σ [mm] 82 vert	n_e	R_{chip}^{peak} [GHz]	R_{chip}^{av} [GHz]	R_{pix}^{max} [kHz]	R_{pix}^{av} [kHz]
standard	11.9	p	6	1.4	1.48	180	0.9	3.5		190	1	0.5	20	10
50 ns	1.89	p	36	25	1.55	3	1.5	3.7						
standard	16.84	p	6	1.4	2.25	180	0.9	3.9						
25 ns	1.33	p	72	25	2.36	3	1.5	3.7		26				
LIU	18.95	p		2	1.69	205	1.0	3.5						
50 ns	3.0	p		25	1.77	3	1.5	3.7						
LIU	28.07	p		2	1.63	205	1.5	4.4						
25 ns	2.22	p		25	1.71	3	1.5	3.7						
HL-LHC		p		2										
BCMS 50 ns	4.09	p		25	2.27	3	1.5	2.8						
HL-LHC	16.25	p		2	1.8	135	1.1	3.7						
BCMS 25 ns		p		25										
ion	0.16	Pb^{54+}	2	15.02	0.7	200	1.2	5.3		610	3	0.2	49	3.4
	0.14	Pb^{54+}	2	1227	1.0	4	1.1	2.9		120	30	0.1	1600	5.6

Table 3: *Summary of LHC beam parameters in PS, together with number of electrons produced per bunch and the hit rate per chip ($R_{chip}^{peak,av}$) and per pixel ($R_{pix}^{peak,av}$.). The $R_{chip}^{peak,av}$ is calculated for horizontal beam size.*

One can see that the horizontal beam size is SD82 is dominated by dispersion. The change of the beam size during the acceleration is very small and it is going to be difficult to conclude about the beam emittance behaviour during this measurement.

4 High-Voltage cage and vacuum chamber

The design of the High-Voltage cage is based on the following assumpotions:

- longitudinal and transverse constraints due to available space,
- electric field quality.

The cage is made of two main electrodes, one housing a detector, and a set of field shaping electrodes. The shaping is done both in transverse and in longitudinal plane.

HV switch grid with a fast switch.

The first aspect to be taken care of is the isolation of the negative electrode. This electrode is expected to be under potential of -20 kV. Its distance from vacuum chamber wall can be estimated by using as a rule a value of 3kV/mm, what gives, for 20 kV a distance of 7 mm.

5 Detector and front-end electronics

5.1 Timepix3-based readout system

5.1.1 Hybrid pixel detector overview

In order to fulfill the requirement of measuring a few hundred electrons representing a single bunch and at a rate of 40 MHz the silicon hybrid pixel detector technology was chosen. It consist of two elements, a pixelated sensor slab and a pixelated readout chip. The sensor is operated with a reverse bias voltage applied across its thickness which establishes a depletion region within the semiconducting material. A charged particle traversing the sensor creates electron-hole pairs along its track through the depletion region. The readout chip, which is bump-bonded onto every pixel of the sensor, collects and converts the freed charges into a voltage. This voltage is then proportional to the deposited particle energy in each pixel. After an ADC stage the hit information is transmitted off the readout chip via a digital high speed interface.

5.1.2 Timepix3 modes of operation

The Timepix3 is currently the most versatile and one of the fastest hybrid pixel detector readout chips available. It was developed within the Medipix Collaboration hosted at CERN and first irradiation measurements have been performed since the

beginning of 2014. The Timepix3 is designed for the same sensor size and pixel number as the previous Timepix1 product of the Medipix Collaboration: 1.4 cm by 1.4 cm ($\approx 2\ cm^2$) and 255 by 255 pixel [5]. The size of one pixel is 55 μm by 55 μm.

Besides measuring deposited energy per pixel this readout chip can also record the arrival time of each hit event and generate immediately a 48 bit data package containing both informations. This is the so called event-based acquisition mode. To improve the SNR and calibrate the chip, every pixel can be set to an individual threshold value. It defines the minimum amount of charge that is necessary to trigger the charge conversion process and time of arrival measurement. Since the deposited energy is measured proportional to a pulse width in time units, the name of this pixel mode is *time-over-threshold* (TOT). The pixel mode that measures the arrival time is called *time-of-arrival* (TOA).

A second acquisition mode is called frame-based, which can be controlled by an external shutter signal that defines the exposure time of the whole chip. As an alternative to recoding TOA and TOT values of single hits per pixel, the number of events with a charge amount over the threshold is counted (historically named *photon counting* - PC) and the integrated total amount of charge (iTOT) is recorded in this mode per pixel during a defined time period.

5.1.3 Timepix3 readout speed limits

Hybrid pixel detectors with a digital readout interface like the Timepix3 consist of an analoge front-end and digital back-end to distribute the recorded hit data. Both parts impose max. speed constraints on the readout possibilities in a specific application of the device.

The predecessor chip, Medipix3, showed a continuous front-end readout capability of about 2 MHz/pixel [6]. Since the Timepix3 front-end is designed for faster pulse processing than that of the Medipix3, an even better performance is expected. However the actual max. count rate per pixel of Timepix3 is not tested yet and needs to be verified with a monochromatic x-ray source in the future. For PS BGI, we need to design the readout system in such a way that we have means to limit the per pixel hit rate to about 2 MHz. The proposal is to use a gating grid in front of the sensor. Once it is active, the electrons will be collected by a potential applied on the wire grid instead of reaching the detector below. If the max. hit rate would be surpassed, the pulse processing of these pixels in the front-end would stall. The result would be a steady overflow of the TOT and TOA values in the corresponding pixels rendering the readout data unusable.

The second readout limit stems from the digital part that drives the chip interface links. The Timepix3 uses eight low voltage differential data lines (SLVS type) plus one clock line to distribute the recorded hit data. In the nominal max. speed configuration these lines can transmit at a gross rate of 640 Mbit/s (using 320 MHz bit clock and DDR encoding) resulting in 5.12 Gbit/s of generated data with an 8b/10b line encoding per Timepix3 chip. Divided by 2^{16} pixels per chip with a

net size per pixel data packet of 48 bits this corresponds to an average hit rate of 85 Mhits/s/chip or 42.5 Mhits/s/cm^2. This means, in the case of a 40 MHz bunch timing, two hits can be recorded per bunch and per chip in the event-based acquisition-mode, requiring no external trigger. To accumulate a whole bunch profile in this mode the hits of several turns must to be average.

With a fixed data package size of 48 bits, the nominal transmit time of one packet containing hit data equals to about 12.5 ns. This is true for any acquisition mode of Timepix3 but limits the application for PS BGI specifically in the frame-based acquisition mode. Here a bunch synchronous shutter signal could be used to trigger the recording of hit data of a whole bunch at once. The following acquisition would then be delayed depending on the number of pixels hit multiplied by 25 ns. In this case several of the following bunches or turns will be skipped and not recorded for profile measurements. This could be circumvented by installing multiple detectors along the beam and triggering them in a specific pattern. One or more detectors would be in acquisition mode while others, finished with recording hits, would send their data at the same time. This time-multiplexed readout strategy would exploit the constant ionization process in the residual gas along the beam line (cf. previous calculation of electron yield due to ionization holds true for $l_{det} = 1.4\ cm$ in equation 7).

5.2 Proposed operation modes

Based on the available Timepix3 operating modes, the most adequate modes have been chosen to match the requirements of four example beams, previously listed in Table 3. Table 4 shows the relevant parameters of these beams together with the proposed Timepix3 modes and operating constraints.

beam type	p (std, 50ns) inj.	p (std, 25ns) extr.	Pb54+ inj.	Pb54+ extr.
kinetic energy $[GHz]$	1.4	25	15.02	1227
No. of bunches	6	72	2	2
revolution time $[us]$	~ 2.1	2.1	5.63	2.1
bunch length $[ns]$	180	4	200	**4**
R_{pix}^{max} [1] [kHz]	20	130	49	**1600**
n_e	190	**26**	610	120
readout delay per chip $[us]$	2.3	$\geq 3 \cdot 2.1$ [2]	≤ 5.63 [3]	1.5
bunch profile recovery rate	one bunch every 2nd turn	one bunch every 3 turns	one bunch per turn	one bunch per turn
Timepix3 operation modes	TOT + TOA	TOA only + pile-up counter [4]	counting + iTOT [5]	TOA only [5]
bunch synchronous trigger needed	no	no	yes	no

Table 4: *Beam parameters and proposed Timepix3 operating modes. Limiting values are emphasized.*

The beam parameters cover a broad signal range in terms of n_e, bunch length and R_{pix}^{max}. While for the operation of PS BGI with ion beams we expect more than enough signal, some proton beams will not create enough electron yield per bunch

[1] max. pixel hit rate per bunch
[2] depends on the required confidence interval of the Gaussian
[3] depends on how short the gating grid period can be set
[4] optional gas injection or multiple chips along beam line
[5] gating within bunch or reduction of detection efficiency

to recover the whole bunch profile in one turn. To reconstruct a correct Gaussian from the rest gas ionization of one bunch above one Timepix3 detector assembly we require roughly $n_e \geq 100$. If the signal per bunch is too low we have three options: increase the pressure by gas injection, average the signal over multiple turns or record the electron yield with multiple detectors along the beam. For the stronger ionizing ion beams it will be crucial to restrict R_{pix}^{max} below 2 MHz to avoid continuos pile-up of the charges in the sensor front-end (cf. 5.1.3) with the mentioned gating grid. This would in principle also allow gating of the electrons within a bunch to limit the number of hits that will be detected if the ionization rate is higher than needed. It must be confirmed in lab tests how short the gating period can be set and if there is any electromagnetic influence on the sensor bias voltage when the HV of the grid is switched.

Another option to limit the amount of detected electrons is to lower the detection efficiency of the sensor. This can be done mainly by lowering the bias voltage. In addition, the Timpeix3 chip offers the possibility to set several internal preamplifier bias voltages. One task of the PS BGI readout system will be to maintain a closed-loop control on those values to tune the detection efficiency to the needed performance depending on the beam type that is to be measured.

Apart from the event-based mode we have the possibility to record a complete bunch image in the frame-based acquisition mode using the PC and iTOT mode of Timepix3. The usage of this mode for PS BGI will depend on the abbility generate a shutter signal which is synchronous to the bunch timing and positions in the PS machine. The readout of these whole bunch image frames will take up to several turns, depending on the number of hit pixels. During this time the detector is not able to record further incoming hits which limits bunch-by-bunch operation.

The event-based acquisition mode of Timepix3 doesn't require external triggering. In this mode only averaging of one bunch on a turn-by-turn basis will be possible. But the advantage is that no bunch synchronous trigger signal is need. The TOA and TOT values will be timestamped by the front-end FPGA with a global clock that is synchronized to the orbit system which is tracking the bunches in PS. The recorded profile data of each bunch can then be correlated with the bunch number and position after the acquisition.

5.3 Radiation hardness

The radiation damage to the material can be divided into ionization damage and displacement damage. Ionization damage leads to the release of charges which are trapped in trapping centers afterwards. This can result in contact polarization effects, building of charges on the interface with isolator and parasitic fields within the detector bulk. Ionization damage is done mainly by charged particles and gamma rays.

Displacement damage leads to modification of the crystal structure of the detector. The structures created by the displacement are vacancies and interstitial

atoms.

The Medipix3 chip, the predecessor of Timepix3 fabricated using the same 130 nm CMOS technology, has been reported to be radiation hard. No breakage has been observed up to a dose of 4.6 MGy using an X-ray source and irradiating the chip at room temperature [7].

5.4 Vacuum tests with electron source

First lab tests have been started with a Timepix1 in vacuum to qualify the sensor candidate. A 100 μm thick p-on-n edgeless silicon sensor is bumb-bonded onto the Timepix1 readout chip. The sensor bulk is made of n-type silicon containing p+ doped pixel implants towards the Timepix1 pixel array. Typically, the outer layer of an Si sensor is made of aluminum to spread the bias voltage equally across the plane. Since this would also stop the low-energy electrons we want to measure in PS BGI, our sensor features no metallization on top. Instead it bears a thin n+ doped layer to improve conductivity.

The electron source for the lab is an electron generation plate (EGP) manufactured by Photonis. Once a voltage between 400 and 1000V is applied, it emits electrons from micro fractures in small channels inside the plate based on the electric field emission principle.

6 Surface electronics

Surface electronics shall be installed in racks in building 368.

7 Magnets

Magnets should provide a good field refion of about 5 cm length and 70-140 cm width, in case of horizontal or vertical devices respectively. The uniformity of the field should be better than 10^{-3} (following magnet analysis for LHC, to be verified by tracking simulations). The field strength should be at least 0.2 T. The effect of

the magnet with the monitor on the beam must be compensated by identical dipole with inversted polarity or by lattice orbit corrector magnets.

8 Conclusions

References

[1] H. Refsum, " Design, Simulation and Testing of a 2D Electron Source Based Calibrating System for a Proton Beam Ionization Profile Monitor", CERN thesis 2004.

[2] Fano, U. Ionizing Collisions of Very Fast Particles and the Dipole Strength of Optical Transitions. Physical Review 95, no. 5 (1954): 1198.

[3] Rieke, Foster F., and William Prepejchal. Ionization Cross Sections of Gaseous Atoms and Molecules for High-Energy Electrons and Positrons. Physical Review A 6, no. 4 (1972): 1507.

[4] M. Patecki, "Analysis of LHC Beam Gas Ionization monitor data and simulation of the electron transport in the detector", CERN-THESIS-2013-155

[5] X. Llopart et al., "Timepix, a 65k programmable pixel readout chip for arrival time, energy and/or photon counting measurements", Nuclear Instruments and Methods in Physics Research A 581, 2007, 485494

[6] Erik Frojdh et al., "Count rate linearity and spectral response of the Medipix3RX chip coupled to a 300 μm silicon sensor under high flux conditions", 15th international workshop on radiation imaging detectors, Paris, June 2013

[7] R. Plackett et al., "Measurement of Radiation Damage to 130nm Hybrid Pixel Detector Readout Chips", Topical Workshop on Electronics for Particle Physics, Paris, Sep 2009, pp.157-160